P5R.5 ANLYSIS OF THE MELTING LAYER BY USING 400MHz WIND PROFILER AND 35 GHz DOPPLER RADAR

Nobuhiro Takahashi*, Yasushi Kitamura
National Institute of Information and Communications Technology
and
Koyuru Iwanami
National Institute for Earth Science and Disaster Prevention

1. INTRODUCTION

To understand the microphysical properties in the melting layer is important to improve the rain retrieval algorithms for both active and passive spaceborne microwave sensors. Several melting layer models have been proposed to explain the radar reflectivity factor (Z) profile of the bright band. In this study, the detail structure of the melting layer is analyzed by using a 400 MHz wind profiler (WPR) owned by National institute of Information and Communications Technology (NICT) and a 35 GHz Doppler radar (MP-Ka) owned by National Research Institute for Earth Science and Disaster Prevention (NIED) (Iwanami et al. 2001) in order to examine and improve the melting layer models proposed by Nishitsuji et al. (1983) and Yokoyama and Tanaka (1984) which are planned to be introduced to the Global Satellite Mapping of Precipitation (GSMaP, Okamoto et al, 2005) rain retrieval algorithm.

2. DATA

Data used in this study was obtained in June 2004 at Okinawa Island, Japan during Baiu season. The radars are located at NICT's Ohgimi wind profiler facility (26ºN, 128ºE). Typical stratiform cases on June 2 are selected for the analysis. The 400 MHz wind profiler (WPR) operated five directions including zenith angle with two range resolutions (100 and 150 m) in about 6 minutes intervals. Only zenith pointing high range resolution Doppler spectrum data is used for the analysis. The 35 GHz Doppler radar (MP-Ka) was operated zenith pointing with 50 m range resolution and data was sampled every second integrated for one minutes. This radar provides the reflectivity factor and Doppler velocity data (spectrum data is not available). Since the beams of the both radar don't match each other (WPR's beam width is 3.5º and the MP-Ka's beam width is 0.3º), relatively stable rain cases are selected for the analysis to reduce the uncertainty of beam mismatching. The attenuation and the Mie scattering effects are negligible for WPR, while these effects are significant for MP-Ka. Therefore the attenuation correction of MP-Ka is required. Other than these effects, both radars need absolute calibration for the analysis. In the next section, cross calibration method is described.

Corresponding author address: Nobuhiro Takahashi, National Institute of Information and Communications Technology (NICT), 4-2-1 Nukuikita-machi, Koganei-shi, Tokyo 184-8795 JAPAN; email: ntaka@nict.go.jp

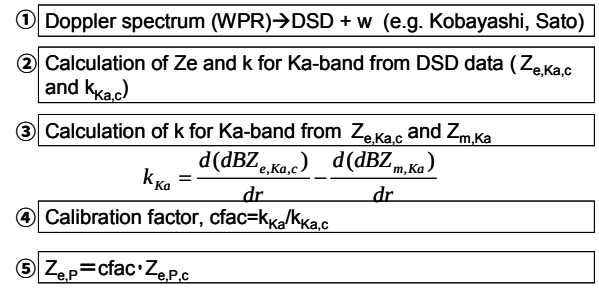

Fig. 1. Flow chart of the cross calibration. Subscripts *Ka* and *P* stand for the frequency and *c* stands for the calculation.

Table 1. Major characteristics of Nishitsuji model.

Item	Note
Major characteristics, assumptions.	Implicitly taking accounts for breakup and coalescence processes.
Volume water fraction (Pw)	Pw is function of height for all sizes. Density = sqrt(Pw)
Fall velocity	Interpolation from fall velocities of snow and rain
DSD (exponential)	Slope parameter (e.g. Λ, D_0) is a function of Pw.
Dielectric constant	Wiener's equation, shape parameter U is given by as a function of Pw (*).

* $$\frac{\varepsilon_s - 1}{\varepsilon_s + U} = P_w \frac{\varepsilon_w - 1}{\varepsilon_w + U} + P_i \frac{\varepsilon_i - 1}{\varepsilon_i + U} + P_a \frac{\varepsilon_a - 1}{\varepsilon_a + U}$$

3. METHODS

3.1 *Cross calibration*

From the spectrum data of the WPR, DSD information below the melting layer is extracted by using an algorithm (e.g. Kobayashi and Adachi, 2005, Sato et al., 1990) that

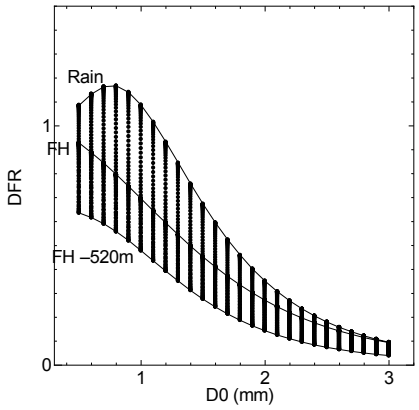

Fig. 2. DFR versus D_0 in the melting layer.

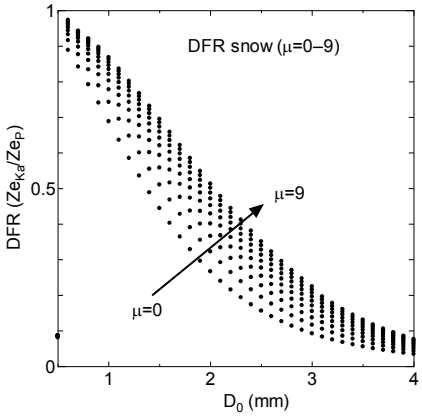

Fig. 3. Same as Fig.2 except for snow and for various shape parameter (μ) in gamma DSD.

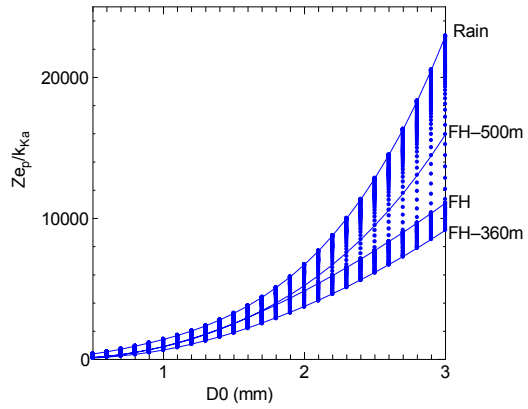

Fig. 4. $Z_{e,P}/k_{Ka}$ versus D_0 in the melting layer.

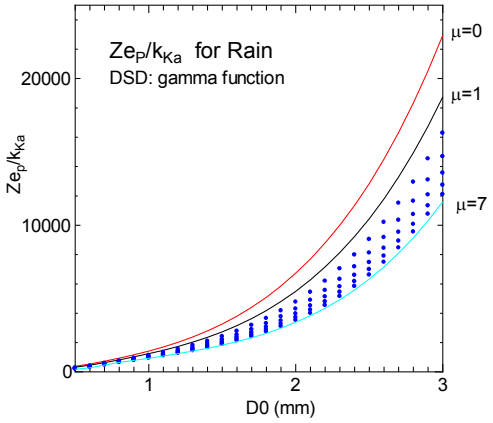

Fig. 5. Ze/k versus D_0 in the rain layer for various shape parameter (μ) in gamma DSD.

first estimates the air motion then the spectra of rain is obtained. The DSD calculated from spectrum data may contain the offset (bias) in the number in each size if the radar is not calibrated. Using DSD information and the Z_m (Measured reflectivity factor, affected by the attenuation) profile of MP-Ka, both radar are calibrated each other. Figure 1 shows the flow chart of calibration procedure.

The effective reflectivity factor and attenuation factor for Ka-band is calculated from the DSD from un-calibrated WPR ($Z_{e,Ka,c}$ and $k_{Ka,c}$, subscript c stands for the calculation). Although the $Z_{e,Ka,c}$ contains bias originated from the calibration effect in the WPR, the vertical gradient ($ddBZ_{e,Ka,c}/dr$), where r is range, cancels this bias. Therefore the attenuation factor of Ka-band radar (k_{Ka}) can be estimated from the $Z_{e,Ka,c}$ and $Z_{m,Ka}$ profiles (see ③ in Fig.1). The ratio of k_{Ka} and $k_{Ka,c}$ is the calibration factor for the WPR. From the corrected $Z_{e,Ka,c}$, offset in MP-Ka measurement including the attenuation in the blind zone and attenuation at the wet antenna is obtained. The corrected Z_e of WPR is compared with the data from the CRL Okinawa bistatic multiparameter radar (COBRA) which is C-band radar developed in 2002 (Nakagawa et al., 2003) and confirmed the validity of the calibration.

3.2 *DSD estimation with the Doppler spectrum*

To estimate the DSD in the melting layer from the Doppler spectrum data, several assumptions are needed such as fall velocity and the back scattering cross section for each particle and height from the freezing level. A melting layer model developed by Nishitsuji et al. (1983) is used for the analysis. This model is developed on the basis of propagation experiments for communication satellites and it implicitly explaining the coalescence/ break-up processes in the model. The major characteristics of this model are listed in Table 1. For the melting layer analysis, model for fall velocity and backscattering cross section are given from the Nishitsuji model then the DSD is calculated from the Doppler spectrum data. One of the critical parameter in the calculation is the freezing height. Rawin sondes launched from the radar site is used to obtain the freezing height. However, the temperature profile around the

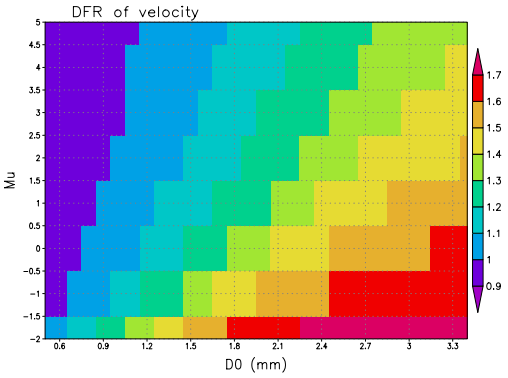

Fig. 6. DFRV value for various D_0 and μ values of gamma distribution.

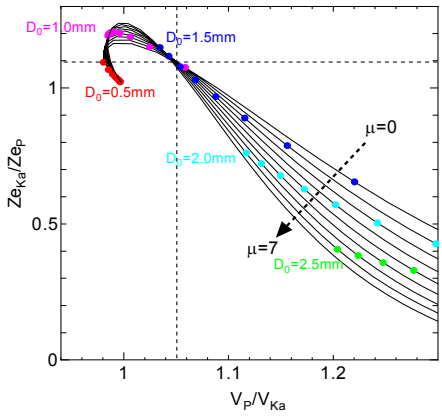

Fig. 7. DFR versus DFRV for various shape parameter in the gamma DSD.

freezing height tends to be uniform; it is difficult to determine the exact freezing height. In the calculation, freezing height was set to the range within a few hundreds meters and DSD is calculated for each freezing height cases. The estimated DSD profile is compare with the DSD in the Nishitsuji model.

Dual frequency method is applied to estimate the DSD profile in the melting layer. The dual frequency ratio (DFR) between 400 MHz and 35 GHz is used to estimate DSD in the melting layer. The DSD is defined as

$$DFR = \frac{Z_{e,Ka}}{Z_{e,P}} = \frac{\int \sigma_{Ka}(D)N(D)dD}{\int \sigma_P(D)N(D)dD},$$

where, $Z_{e,Ka}$ and $Z_{e,P}$ are the effective reflectivity factor of Ka- and P-band, respectively, σ_{Ka} and σ_P are the back scattering cross section of Ka- and P-band, respectively, and $N(D)$ is number concentration. The DFR is a function of median volume diameter (D_0) if the DSD is expressed by gamma distribution, $N(D) = N_0 D^{\mu} \exp(-(3.57+\mu)D/D_0)$. A lookup table between DFR and D_0 is prepared for each height based on the backscattering cross section data in the Nishitsuji model. Once the DFR is obtained the DSD (D_0) is estimated from the lookup table. Figures 2 and 3 show the DFRs for various D_0 in the melting layer (Fig. 2) and snow (Fig. 3). In Fig. 3, DFR for various shape parameter (μ) in gamma DSD are plotted.

Dual frequency techniques other than the DFR method is tested to validate the DSD profile and the calibration. The attenuation factor in the Ka-band can be expressed at the same manner as shown in section 3.1. If $ddBZ_{e,Ka}/dr$ is replaced by $ddBZ_{e,P}/dr$, k_{Ka} is obtained and the ratio between k_{Ka} and $Z_{e,P}$ is expressed as,

$$\frac{Z_{e,P}}{k_{Ka}} = \frac{\int \sigma_P(D)N(D)dD}{\int CQ_{ext,Ka}(D)N(D)dD},$$

where $Q_{ext,Ka}$ is extinction cross section in Ka-band and C is constant. This equation is also function of D_0. Figures 4 and 5 show the relationship between the ratio and D_0 in the melting layer and that in the rain layer for various μ.

The ratio of the Doppler velocity of both frequencies is also useful to estimate the DSD in the rain layer. The dual frequency ratio of the Doppler velocity (DFRV) is expressed as,

$$DFRV = \frac{V_{Ka}}{V_P} = \frac{\int (V(D)+w)\sigma_{Ka}(D)N(D)dD \int \sigma_P(D)N(D)dD}{\int \sigma_{Ka}(D)N(D)dD \int (V(D)+w)\sigma_P(D)N(D)dD}.$$

If the w is negligible and the $V(D)$ is expressed by power law, (e.g. $V(D)=3.778D^{0.67}$), DFRV is written as,

$$DFRV = \frac{1}{DFR} \cdot \frac{\int D^{0.67}\sigma_{Ka}(D)D^{\mu}\exp(-(3.67+\mu)D/D_0)}{\int D^{0.67}\sigma_P(D)D^{\mu}\exp(-(3.67+\mu)D/D_0)}.$$

The second term in the right hand side is same as DFR except for weighted by $D^{0.67}$. Therefore, the DFRV shown in Fig. 6 is expected to be near unity and DFRV shows similar tendency to the DFR in Fig. 3. Figure 7 shows the relationship between DFR and DFRV. This figure shoes that D_0 is strongly depend on μ that indicates the difficulty to use this method. This figure also shows that DFRV of 1.05 is independent on μ. It indicates that this value can be used for the relative calibration between two frequencies.

3.3. *DSD estimation above FH*

Two approaches are combined to estimate the DSD above the FH. First method is the DFR method, since the DFR for snowfall is relatively linear curve; D_0 is more reliable (Liao et al., 2003, see also Fig. 3). In addition,

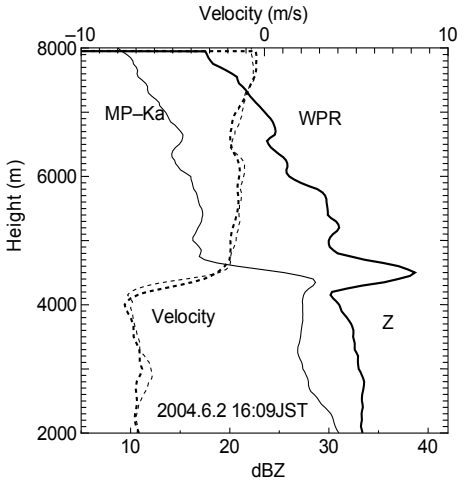

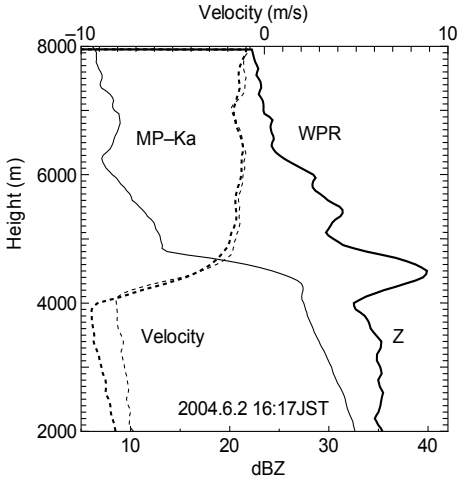

Fig. 8. Vertical profiles of Z (solid lines) and Doppler velocity (dashed lines) from WPR (bold) and MP-Ka (thin), at 16:09 UT (top) and at 16:17 UT (bottom) on June 2, 2004.

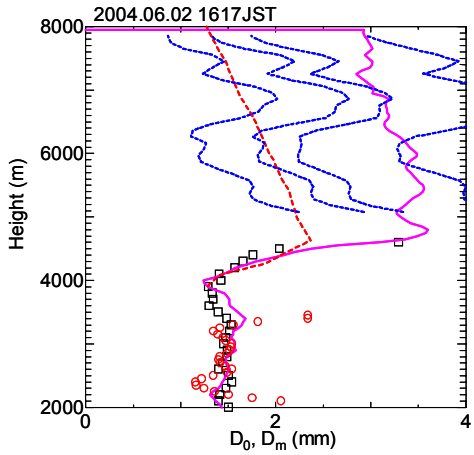

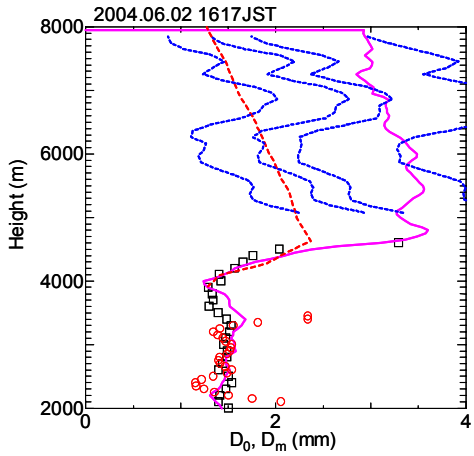

Fig. 9. D_0 and D_m profiles of the cases in Fig. 8 obtained from the spectrum data (open squares in the rain and melting layer and dashed lines above the melting layer by several fall velocity models), DFR method (solid lines), and $Z_{e,P}/k_{Ka}$ method (open circles). The DSD model of the Nishitsuji model is also shown by red dashed lines.

attenuation is not significant for snowfall; it leads the more stable solution in the DFR method.

The second method is to use the Doppler spectrum. The issue in this method is that the width of the spectra is much narrower than the rain spectra and the fall velocity of snow varies with the shape and density. In this study, several fall velocity models and density models are tried and the appropriate fall velocity model is searched by comparing the D_0 from both methods.

4. RESULT

Figure 8 shows Z and Doppler velocity profiles from WPR and MP-Ka of two typical stratiform rain (16:09UT and 16:17UT on June 1). The Z profile of WPR is calibrated by the method described in Section 3.1. The case at 16:09UT shows relatively weaker Z than the case at 16:17UT: significant attenuation is seen in MP-ka profile at 16:17UT. This is consistent with the Doppler velocity profile; larger difference appears at 16:17UT while almost identical profile is seen at 16:09UT in rain layer.

The Z profile in the melting layer shows clear contrast; clear peak is not seen in MP-Ka because of the large attenuation and the Mie scattering effect. The Doppler velocity profile in the melting layer is very complicated structure especially at 16:17UT; at the upper layer in the melting layer, the Doppler velocity of MP-Ka is larger than that of WPR, the Doppler velocity of WPR become larger than that of MP-Ka as the height goes lower. It can be explained by that the smaller particles which melt faster than larger particle has higher fall velocity. It is not explained by the Nishitsuji model. The melting layer

model by Yokoyama and Tanaka (1984) may explain the Doppler velocities in the melting layer; smaller drops which melt faster than larger particles can show faster fall velocity in the model. In the following analysis on the melting layer, Doppler velocity data is not used. Above the melting layer, significant attenuation cannot be seen in MP-Ka.

The DSD profiles of the cases in Fig. 8 are retrieved by the method explained in section 3. Figure 9 shows the DSD profile. At the rain layer, two dual frequency methods are examined by referring the mass weighted diameter (D_m) from spectrum to find the appropriate parameter for the dual frequency analysis (e.g. calibration offset and μ). Comparing two dual-frequency methods, the method using *Ze/k* is more stable than the DFR method. However, this method requires significant attenuation in the higher frequency and the distance to obtain the gradient of *Z*.

The DFR method is used for the melting layer analysis. It starts the rain layer to have same D_0 in the rain layer and the D_0 in the melting layer is calculated. In Fig. 9, both from the DFR method and spectrum calculation show similar D_0 profile in the melting layer at both 16:09UT and 16:17UT. The D_0 in the melting layer is, however, much larger than the D_0 used in the Nishitsuji model (red dashed lines in Fig. 9). This result implies that the DSD in the Nishitsuji model should be revised.

Above the freezing height, the DFR method is used to estimate the DSD. Not only the DSD but also the snow density is crucial in the retrieval in the snow layer (above freezing height), snow fall velocity model is examined by using the spectrum data and the DFR method as explained in Section 3. In Fig. 9, smaller DSD is obtained from the faster fall velocity model and the model which has same D_0 with that from the DFR method will give the solution of D_0. However, the DSD profile from spectrum data shows larger fluctuation with height. This result reminds the effect of the air motion. If we assume the D_0 changes monotonically with height, the deviation from the monotonic line may be the air motion: negative deviation expresses the upward motion and positive deviation is downward motion. Based on these assumptions, up draft appear at 6 km in height and the fall velocity slightly reducing with height.

5. SUMMARY

In this study, dual frequency radar observation data is used to analyze the melting layer as well as the rain and snow layer, especially for the DSD parameter. The result shows D_0 value from the analysis is larger than the Nishitsuji model. It must be examined by other measurements such as COBRA data. Only two cases are analyzed in this study, more cases are needed to evaluate the DSD in the melting layer and other parameters such as thickness of the melting layer.

6. ACKNOWKEGEMENTS

This work is conducted as a part of the Global Satellite Mapping of Precipitation (GSMaP) project supported by the Core Research for Evolutional Science and Technology (CREST) program of Japan Science and Technology Agency (JST).

7. REFERENCES

Iwanami, K., R. Misumi, M. Maki, T. Wakayama, K. Hata, and S. Watanabe, 2001: Development of a multiparameter radar system on mobile platform, *Proc. 30th Conf. on Radar Meteor.*, Ame. Meteor. Soc., 104-106.

Kobayashi, T., and A. Adachi, 2005: Retrieval of arbitrary shaped raindrop size distributions from wind profiler measurements, *J. Atmos. and Oceanic Technol.*, **22,** 433–442.

Liao, L. and R. Meneghini, T. Iguchi and A.Detwiler, 2003: Validation of snow parameters as derived from dual-wavelength airborne radar, *Proc. 31st Conf. Radar Meteor.*, Ame. Meteor. Soc.,411-414.

Nakagawa, K., H. Hanado, S. Satoh, N. Takahashi, T. Iguchi and K. Fukutani, 2003: Development of a new C-band bistatic polarimetric radar and observation of typhoon events, *preprints 31st Conf. on Radar Meteor.*, Seattle, 863-866**.**

Nishitsuji, A., M. Hoshiyama, J. Awaka, and Y. Furuhama,1983: An analysis of propagative character at 34.5 GHz and 11.5 GHz between ETS-II satellite and Kasima station. - On the precipitation model from stratus, *IEICE Trans. (Japanese Edittion),* **Vol. J66-B**, 1163-1170. (*in Japanese*)

Okamoto, K., T. Ushio, T. Iguchi, N. Takahashi and K. Iwanami, 2005: The Global Satellite Mapping of Precipitation (GSMaP) Project. *IGARSS 2005*, Seoul.

Sato, T., H. Doji, H. Iwai, I. Kimura, S. Fukao, M. Yamamoto, T. Tsuda and S. Kato, 1990: Computer processing for deriving drop-size distributions and vertical air velocities from VHF Doppler radar spectra, *Radio Sci.* , **Vol.25, No.5,** pp.961-973,.

Yokoyama, T., and H. Tanaka, 1984: Microphysical processes of melting snowflakes detected by two-wavelength radar. Part I. Principle of measurement based on model calculation, *J. Meteor. Soc. Japan*, 650-667.